Parametric Optimization of a Three-Phase MCR WPT System With Cylinder-Shaped Coils Oriented by Soft-Switching Range and Stable Output Power

Fuxin Liu, *Senior Member, IEEE*, Ze Ding, Xiewei Fu, and Ralph M. Kennel, *Senior Member, IEEE*

***Abstract*—Multi-phase magnetically coupled resonant (MCR) wireless power transfer (WPT) technology can fulfill the requirements of time-varying spatial positions of loads in mid-range applications, as it can generate a rotating magnetic field around sending coils, and effectively reduce the limits of spatial positions on transfer characteristics including output power and transfer efficiency. Nevertheless, the design of coils parameters and control strategies put a great influence on the realistic transfer characteristics, which should be considered elaborately in practice. In this paper, a three-phase MCR WPT system with cylinder-shaped coils is investigated, the equivalent circuit model is built to carry out the theoretical analysis. Based on that, the influence on zero-voltage-switching (ZVS) conditions of power switches and the output power of the system, resulting from different phase-shifted angles between each phase, coil turns and angular misalignments of the receiving coil, is analyzed comprehensively. Detailed discussions on relationships among coil turns, the angular misalignment, ZVS conditions, and the output power are completed under different phase-shifted angles. Furthermore, the parametric optimization of coil turns, as well as phase-shifted angles, are proposed to ensure the power switches realize ZVS and ensure the system realize stable output power within the full range of angular misalignment. Finally, experiments are carried out to evaluate the accuracy of theoretical analysis and confirm the validity of the proposed optimal design.**

***Index Terms*—Angular misalignment, magnetically coupled resonant (MCR), output power characteristics, three phase, wireless power transfer (WPT), zero-voltage-switching (ZVS).**

I. Introduction

WIRELESS power transfer (WPT) is a promising technology that has been investigated in various forms, contexts and for diverse applications. An increasing number of various solutions for powering and charging devices in a cordless manner has been proposed, ranging from applications such as portable electronics to electrical vehicles, as well as biomedical implants, etc. [1]–[4]. Recently, magnetically coupled resonant (MCR) WPT has drawn significant interest for implementing the near-field WPT due to its high transfer efficiency as well as long transfer range. Furthermore, MCR WPT effectively avoids the power leakage to non-resonant externalities and thus ensures safety to the neighboring environment [5], [6].

However, among other constraints, the system performance, which most commonly is measured by the output power capability and transfer efficiency, considerably limits the range of such applications. Usually, the output power and transfer efficiency are restricted to limited distances and spatial dimensions, as the mutual coupling between sending and receiving coils will attenuate accordingly along with increasing lateral and/or angular misalignments. It is an urgent issue to be addressed that how to realize an omni-directional power transfer for MCR WPT systems and enable the loads to receive power under any misalignment between sending and receiving coils [7]–[10].

For this purpose, multi-phase WPT techniques was proposed to intend to generate a rotating magnetic field covering all the directions around the sending coils [11]–[17], among which, an omni-directional MCR WPT system with two-phase orthogonal coils was investigated, and the statement is made that the omni-directional WPT would not be realized in any case if the two-phase orthogonal coils are driven by the currents in phase [11], [12]. Furthermore, to extend the power transfer range in spatial scales, three-phase orthogonal coils were proposed in MCR WPT systems, serving as both sending and receiving coils, as well as the effective control methods to create a rotating magnetic field, which attempts to realize the genuine omni-directional power transfer [15]–[17]. Although multi-phase orthogonal coils are effective to provide power to the load continuously under time-varying spatial misalignments, the magnitude of current flowing through the two- or three-phase sending coils behaves much higher than the counterparts in single-phase systems at same power level, meanwhile, the two- and three-dimension spherical configurations put forward higher requirements of the spatial dimension. It also should be noticed that the systems in the above literatures are mostly driven in a current-fed manner, which is not easily designed and implemented in practice.

The ongoing researches demonstrate that the performance of MCR WPT systems is highly relevant to the system parameters, including the coil profile, coil turns, and controlled variables, etc., thus it will provide an opportunity to optimize the

Manuscript received February 25, 2019; accepted April 22, 2019. Date of publication April 29, 2019; date of current version October 18, 2019. This work was supported in part by the National Natural Science Foundation of China under Grant 51877103, in part by the Fundamental Research Funds for the Central Universities, China, under Grant NS2018020, and in part by Jiangsu Province University Outstanding Science and Technology Innovation Team Project. This paper was presented in part at the IEEE Applied Power Electronics Conference and Exposition, Tampa, FL, USA, March, 2017, and in part at the IEEE Energy Conversion Congress and Exposition, Cincinnati, OH, USA, October 2017. Recommended for publication by Associate Editor S. K. Panda. *(Corresponding author: Fuxin Liu.)*

F. Liu, Z. Ding, and X. Fu are with the College of Automation Engineering, Nanjing University of Aeronautics and Astronautics, Nanjing 210016, China (e-mail: liufuxin@nuaa.edu.cn; dize1995.dize.1995@qq.com; fuxiewei@nuaa.edu.cn).

R. M. Kennel is with the Department of Electrical and Computer Engineering, Technical University of Munich, 80333 Munich, Germany (e-mail: ralph.kennel@tum.de).

Color versions of one or more of the figures in this paper are available online at http://ieeexplore.ieee.org.

Digital Object Identifier 10.1109/TPEL.2019.2914154

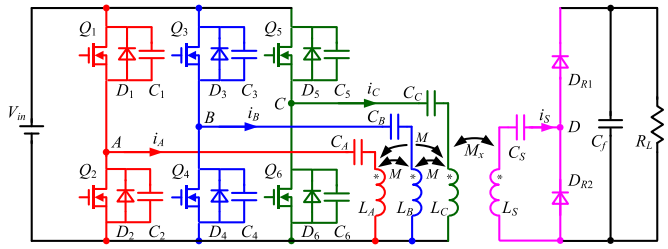

Fig. 1. Topology of three-phase MCR WPT system.

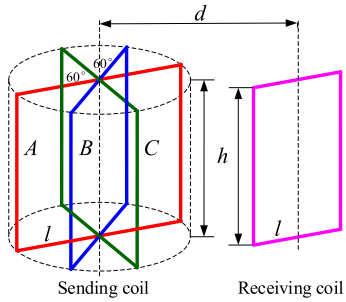

Fig. 2. Stereogram of coil configuration.

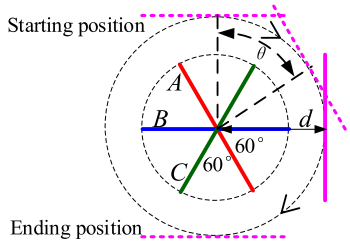

Fig. 3. Planform of coil configuration.

above parameters to achieve superior output power characteristics and high overall system efficiency [18]–[22]. For example, in [18], the comprehensive analysis was performed on the driver inverter of single-phase MCR WPT system to realize zero-voltage-switching (ZVS) for power switches, and it is found that ZVS conditions were directly related to the resonant coupled circuit. However, how to design the resonant coupled circuit was not considered. In [19], a trifoliate coil configuration was adopted in a three-phase magnetically coupled inductive WPT system to improve the system efficiency tolerance to the lateral and angular misalignments of loads. In [20], an optimization method on coil turns was presented in single-phase MCR WPT system under variable spatial scales to determine the optimized coupling range between the receiving coil and the sending coil, within which the output power of the system can always maintain constant.

In this paper, a three-phase MCR WPT system with cylinder-shaped coils will be elaborated to satisfy the requirements of compact space and cut down the rated current flowing through sending coils due to the inherent mutual coupling between coils. The equivalent analytical model of the system with voltage-fed excitation is built to evaluate the influence on the mutual inductance, ZVS conditions of power switches, and the output power, caused by angular misalignment of loads, phase-shifted angles between each phase, and coil turns. Based on theoretical analysis, the optimal range of coil turns and phase-shifted angles is obtained by the mathematical calculation, which ensures not only all the switches achieve ZVS within the full range of angular misalignment, but also the system realize the optimal output power characteristics that features high amplitude and low fluctuation. Finally, a prototype had been built and tested to validate the theoretical analysis.

II. Modeling and Analysis of Three-Phase MCR WPT System

A. Topology of Three-Phase MCR WPT System

Fig. 1 shows the topology configuration of the three-phase MCR WPT system, where the resonant tank of each phase is driven by a half-bridge inverter sharing a common dc input voltage. The inducing voltage on the receiving coil is rectified by a voltage doubler rectifier. L_A, L_B, L_C, and L_S are the self-inductors of three-phase sending coils and the receiving coil. C_A, C_B, C_C, and C_S are compensated capacitors in the resonant tanks of phase *A*, *B*, *C,* and the receiving side, respectively. *M* is the mutual inductance between the sending coils. M_x $(x = A, B, C)$ are the mutual inductances between the receiving coil and sending coils. Fig. 2 shows the stereogram of the three-phase cylinder-shaped coil configuration, which is composed of three sending coils and one receiving coil. All the sending coils are uniform rectangular coils, in which, the angle between any two sending coils is 60°. The shape and dimension of the receiving coil are same as sending coils, and the distance between their central axes is *d*.

B. Mutual Inductance Model of Three-Phase MCR WPT System

Generally, the mutual inductance M_x changes along with the spatial locations of coils, which will exert an influence on the output power and transfer efficiency, thus it is necessary to build the accurate mutual inductance model for theoretical analysis. In this paper, only one kind of spatial locations, i.e., the rotating angular misalignment between the receiving coil and sending coils, is considered for simplicity. Fig. 3 shows the planform of coil configuration, in which, θ is the angular misalignment. It is assumed that the receiving coil always rotates clockwise around sending coils, being tangent with the dashed circle, and the plane of the receiving coil is parallel with the central axis of sending coils. The variation range of θ is 0°∼180° due to the symmetric structure of coils. M_x can be calculated by solving the double integral in Neumann's formula

$$M_x = \frac{\mu_0 N_P N_S}{4\pi} \oint \oint \frac{\mathbf{dl_P} \cdot \mathbf{dl_S}}{r_{PS}} \tag{1}$$

where N_P, N_S, $\mathbf{l_P}$, $\mathbf{l_S}$, $\mathbf{dl_P}$, and $\mathbf{dl_S}$ are the coil turns, the length vector of each turn, and the infinitesimal of sending coils and the receiving coil, respectively. r_{PS} is the distance between $\mathbf{dl_P}$ and $\mathbf{dl_S}$. μ_0 is the magnetic permeability of vacuum.

Considering the fixed position of three-phase sending coils, the mutual inductances between sending coils are constant and can be calculated by (1) [23]. Fig. 4 shows the curves of M_{0x} between the receiving coil and sending coils derived from (1) provided that all coil turns are one, where the specifications of coils are listed as follows: $l = 22$ cm, $h = 30$ cm, $d = 25$ cm. From Fig. 4, it can be known that M_{0A}, M_{0B}, and M_{0C} vary along with the angular misalignment in an interleaved manner, and the interleaved angular difference is 60°.

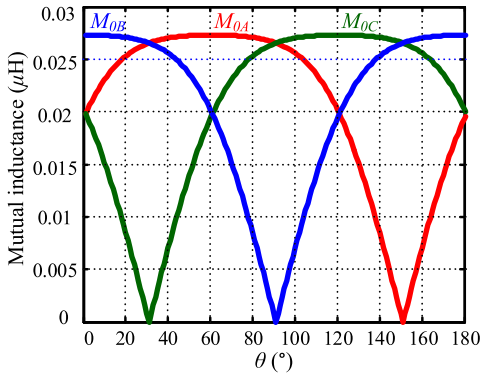

Fig. 4. Curves of mutual inductance M_{0x}.

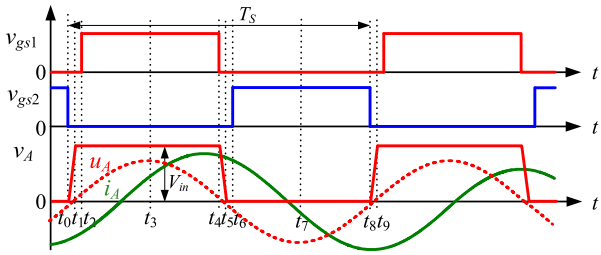

Fig. 5. Key waveforms in phase *A*.

C. Equivalent Circuit Model of Three-Phase MCR WPT System

In the three-phase half-bridge inverter, each bridge is controlled independently and the dual power switches in one bridge are turned ON/OFF alternately with same duty cycle and an introduced small dead time. In this paper, the fundamental harmonic analysis (FHA) method is adopted to derive the equivalent circuit model in the steady state.

Fig. 5 depicts key voltage and current waveforms in phase *A*. v_{gs1} and v_{gs2} are the gate-drive voltages of power switches. v_A and i_A are the exciting square-wave voltage and the resonant current in phase *A*, respectively. u_A is the fundamental harmonic component of v_A. Based on the FHA method, v_A can be decomposed with Fourier series expansion method

$$v_A(t) = \frac{V_{\text{in}}}{2} + \frac{2V_{\text{in}}}{\pi} \sum_{n=1,3,5\cdots} \frac{1}{n} \sin(n\omega t) \tag{2}$$

where, V_{in} is the dc input voltage, ω is switching angular frequency, and $\omega = 2\pi f_s$, f_s is the switching frequency. From (2), v_A is composed of a dc component and a series of ac components at different frequencies. It should be noted that only the ac components can resonate in the resonant tanks.

The fundamental harmonic component of v_A is defined as

$$u_A(t) = \frac{2V_{\text{in}}}{\pi} \cos\left(\omega t + \frac{\pi}{2}\right). \tag{3}$$

In this paper, the phase angle control strategy is adopted to generate the required rotating magnetic field [15], and the expressions of three-phase equivalent input voltages are defined as

$$u_A(t) = \frac{2V_{\text{in}}}{\pi} \cos\left(\omega t + \frac{\pi}{2}\right)$$

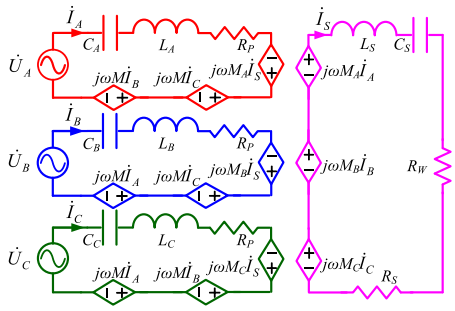

Fig. 6. Decoupled equivalent circuit of the system.

$$u_B(t) = \frac{2V_{\text{in}}}{\pi} \cos\left(\omega t + \frac{\pi}{2} + \varphi\right)$$
$$u_C(t) = \frac{2V_{\text{in}}}{\pi} \cos\left(\omega t + \frac{\pi}{2} + \alpha\right) \tag{4}$$

where, φ and α are the introduced phase-shifted angles between each phase.

The relationship between the equivalent load resistance R_W and the real load resistance R_L is

$$R_W = \frac{2}{\pi^2} R_L. \tag{5}$$

Fig. 6 shows the decoupled equivalent circuit of the system derived from Fig. 1, where the mutual couplings between coils are equivalent to the current-controlled voltage sources. From Fig. 6, one can obtain

$$\begin{bmatrix} \dot{U}_A \\ \dot{U}_B \\ \dot{U}_C \end{bmatrix} = \begin{bmatrix} Z_p & j\omega M & j\omega M \\ j\omega M & Z_p & j\omega M \\ j\omega M & j\omega M & Z_p \end{bmatrix} \begin{bmatrix} \dot{I}_A \\ \dot{I}_B \\ \dot{I}_C \end{bmatrix} - \begin{bmatrix} j\omega M_A \\ j\omega M_B \\ j\omega M_C \end{bmatrix} \left[\dot{I}_S\right] \tag{6}$$

$$[0] = \begin{bmatrix} j\omega M_A & j\omega M_B & j\omega M_C \end{bmatrix} \begin{bmatrix} \dot{I}_A \\ \dot{I}_B \\ \dot{I}_C \end{bmatrix} - [Z_S] \left[\dot{I}_S\right] \tag{7}$$

where Z_p and Z_S are the equivalent impedance of sending coils and the receiving coil.

To simplify the analysis, the following assumptions are made.

1) Resonant inductors $L_A = L_B = L_C = L_S$, compensated capacitors $C_A = C_B = C_C = C_S$. The switching frequency equals to the resonant frequency.
2) Resistance of coils $R_P = R_S$, and they are assumed to be constant.
3) Coil turns $N_P = N_S = N$.

Meanwhile, $L_x\,(x = A, B, C, S)$ and $C_x\,(x = A, B, C, S)$ are designed to resonate with each other, i.e.,

$$j\omega L_x + \frac{1}{j\omega C_x} = 0. \tag{8}$$

Under the resonant state, the equivalent impedance, Z_p and Z_S can be expressed by

$$Z_P = R_P + j\omega L_x + \frac{1}{j\omega C_x} = R_P \tag{9}$$

$$Z_S = (R_S + R_W) + j\omega L_S + \frac{1}{j\omega C_S} = R_S + R_W. \tag{10}$$

To further simplify (6) and (7), one can assume that

$$\mathbf{U} = \begin{bmatrix} \dot{U}_A & \dot{U}_B & \dot{U}_C \end{bmatrix}^T \tag{11}$$

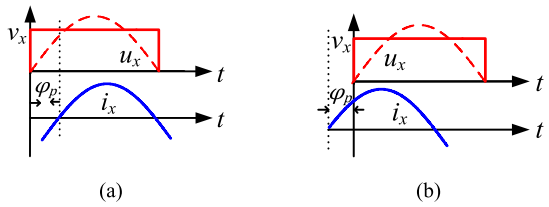

Fig. 7. Definition of φ_P. (a) $\varphi_P \le 0$. (b) $\varphi_P > 0$.

$$\mathbf{I} = \begin{bmatrix} \dot{I}_A & \dot{I}_B & \dot{I}_C \end{bmatrix}^T \tag{12}$$

$$\mathbf{A} = \begin{bmatrix} R_P & j\omega M & j\omega M \\ j\omega M & R_P & j\omega M \\ j\omega M & j\omega M & R_P \end{bmatrix} \tag{13}$$

$$\mathbf{B} = \begin{bmatrix} j\omega M_A & j\omega M_B & j\omega M_C \end{bmatrix}. \tag{14}$$

Therefore, (6) and (7) can be simplified as

$$\mathbf{U} = \mathbf{A} \cdot \mathbf{I} - \mathbf{B}^{\mathbf{T}} \cdot \dot{I}_S \tag{15}$$

$$[0] = \mathbf{B} \cdot \mathbf{I} - Z_S \cdot \dot{I}_S. \tag{16}$$

From (15) and (16), the three-phase resonant currents **I**, the output current $\dot{I}_S$, and the output power P_{out}, are given by

$$\mathbf{I} = Z_S\left(Z_S\mathbf{A} - \mathbf{B}^T\mathbf{B}\right)^{-1}\mathbf{U} \tag{17}$$

$$\dot{I}_S = \mathbf{B}\left(Z_S\mathbf{A} - \mathbf{B}^T\mathbf{B}\right)^{-1}\mathbf{U} \tag{18}$$

$$P_{\text{out}} = Re\left(R_W \cdot \dot{I}_S \cdot \dot{I}_S^*\right). \tag{19}$$

From above equations, it can be known that the phase-shifted angles, the mutual inductances, and the load are the dominant influential factors upon the three-phase resonant currents and the output power. In the following, we will focus on the optimization of coils to adjust the mutual inductances, and modulate the phase-shifted angles to achieve a superior performance for the system.

III. Optimization of Coils and Phase-Shifted Angles for ZVS Range

In the three-phase MCR WPT system, it is necessary to achieve soft switching for the driver inverter to improve the overall system efficiency and avoid the distortion of resonant current and electromagnetic interference noises resulted from the hard switching on power switches, as the system always operates with high switching frequency. It is well-known that to realize ZVS for the driver inverter, it is essential to ensure the resonant currents lag to the fundamental components of the equivalent input voltages (i.e., corresponding driving signals) in same phase before the switches turn on. Due to different system parameters and operation conditions, it is hard but possible to realize soft switching for all the switches within full angular misalignment. Assuming that the profiles of coils are determined and the coil turns can be adjusted, in the following, the parameters optimization on coil turns and phase-shifted angles to fulfill ZVS for switches will be discussed in detail.

Fig. 7 shows the waveforms of the resonant current and the corresponding equivalent input voltage in same phase, where u_x $(x = A, B, C)$ represents the fundamental harmonic component of v_x, and the phase difference between i_x and u_x is

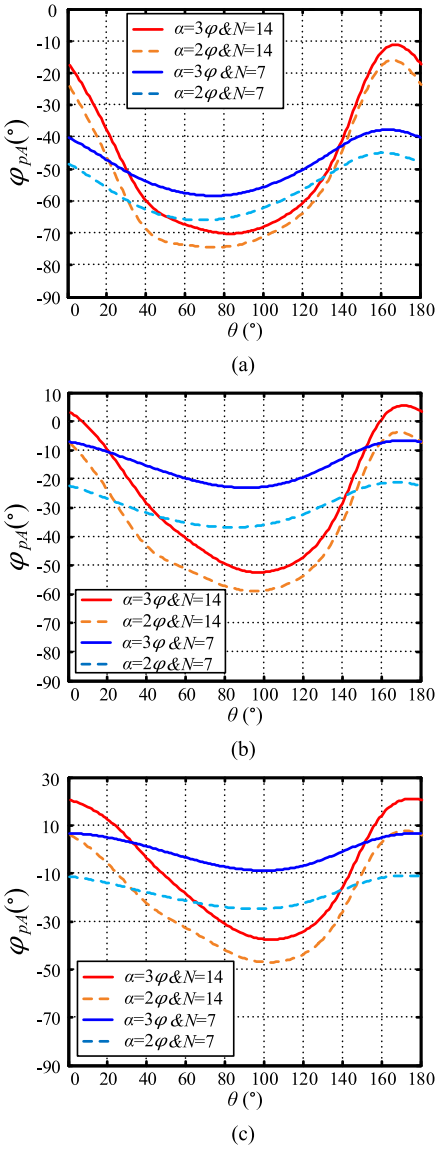

Fig. 8. Curves of φ_{PA} as a function of θ and N under specific φ and α. (a) $\varphi = 10°$. (b) $\varphi = 20°$. (c) $\varphi = 30°$.

defined as the soft-switching angle φ_P, which is given by

$$\varphi_P = \frac{\pi}{2} - |\varphi_x| \tag{20}$$

where φ_x is the phase of resonant currents. Obviously, when $\varphi_P \le 0$ [see Fig. 7(a)], i_x lags to u_x and flows through the body-diodes before the switches turn on, thus ZVS can be achieved. Otherwise, the switch will suffer hard switching when $\varphi_P > 0°$ [see Fig. 7(b)].

From (17), φ, α, θ, and N directly correlate with the phase and magnitude of resonant currents i_A, i_B, and i_C, and further influence on φ_P, which manifests that it is greatly complicated to analyze ZVS range if all the parameters are considered simultaneously. However, if φ and α are determined to meet the pre-designed constraint conditions and be constant beforehand, thus φ_P can be simplified as the function of θ and N. For this purpose, the relationship between φ and α is classified into three cases in this paper: (a) $\alpha = \varphi$; (b) $\alpha = 2\varphi$; (c) $\alpha = 3\varphi$. If $\alpha = \varphi$, the output power will fluctuate severely regardless of coil turns,

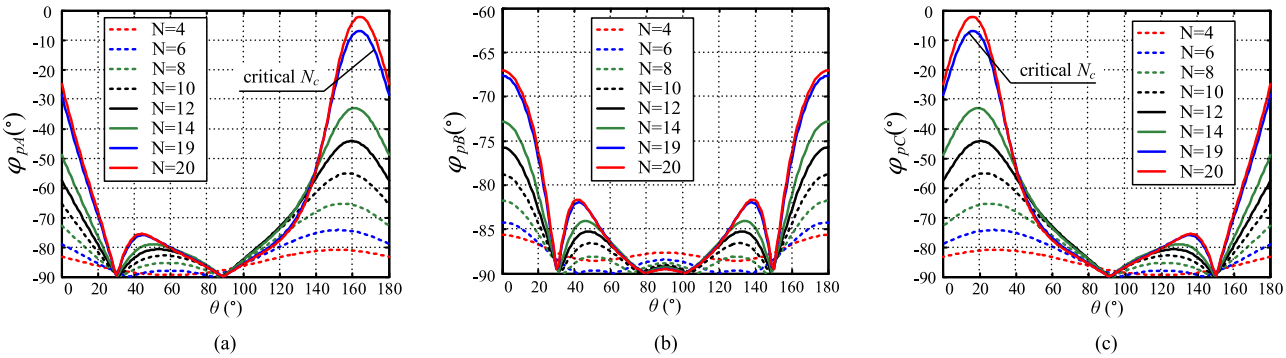

Fig. 9. Curves of φ_P against θ and N when $\varphi = 0°$, $\alpha = 0°$. (a) Phase A. (b) Phase B. (c) Phase C.

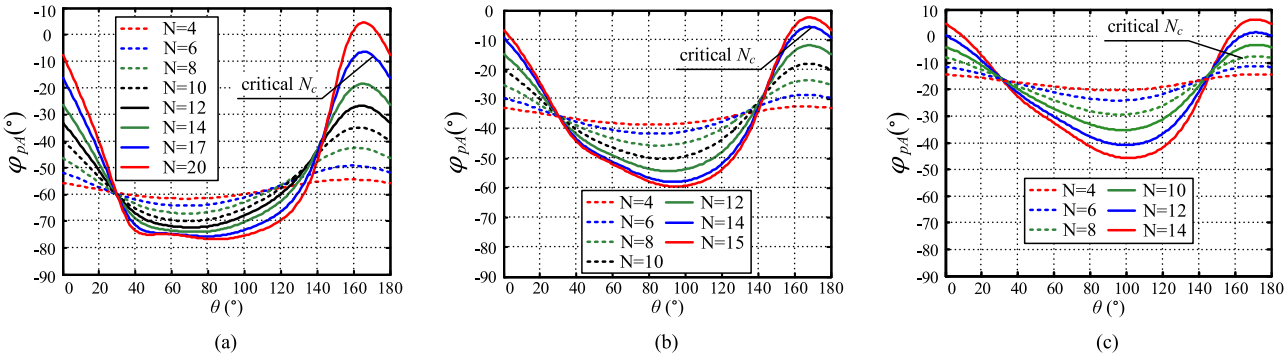

Fig. 10. Curves of φ_P in phase A against θ and N. (a) $\varphi = 10°$, $\alpha = 20°$. (b) $\varphi = 20°$, $\alpha = 40°$. (c) $\varphi = 30°$, $\alpha = 60°$.

which will be analyzed in Section IV, thus this case will not be discussed in this section. Fig. 8 shows the curves of φ_P in phase A, φ_{PA}, as a function of θ and N under specific φ and α. As depicted in three subgraphs, φ_{PA} in the case of $\alpha = 2\varphi$ is always smaller than the case of $\alpha = 3\varphi$ under any coil turns and angular misalignments. As ZVS can only be realized when $\varphi_P \leq 0$, and will be much easier to be achieved if φ_P is much less than zero, which means ZVS range in the case of $\alpha = 2\varphi$ will be obviously wider than the case of $\alpha = 3\varphi$. Therefore, in the following, the constraint between φ and α is determined as $\alpha = 2\varphi$.

On the premise that $\alpha = 2\varphi$, Fig. 9 illustrates the curves of φ_P in each phase against θ with increasing N when $\varphi = 0°$, $\alpha = 0°$, from which, the maximum φ_P increases along with N if θ is constant. Specifically, Fig. 10 shows the curves of φ_{PA} against θ and N when $\varphi = 10°$, $\varphi = 20°$, and $\varphi = 30°$, respectively, the maximum φ_{PA} also increases with N. However, φ_P always reaches maximum and possibly approach zero when θ changes within 0°∼20° and 160°∼180°, as shown in Fig. 10(c), which means the switches will lost ZVS. Therefore, to ensure ZVS operation for the switches, the boundary value of φ_P is designed as $-5°$ that corresponds to a critical coil turns N_c, as labeled in each subgraph. Fig. 11 shows the curve of N_c versus different φ, from which, N_c decreases when φ increases, and it is impossible to realize ZVS for power switches when $\varphi > 40°$ as N_c will be negative. Therefore, if $\varphi < 40°$, all the power switches can realize ZVS if the coil turns are designed according to the range of N_c.

As a conclusion, to achieve ZVS in the driver inverter under any angular misalignment, the constraint between φ and α should be $\alpha = 2\varphi$, and the maximum φ must be less than 40°. The specific coil turns will be designed according to the other optimization objective, i.e., stable output power characteristics, which will be analyzed in Section IV.

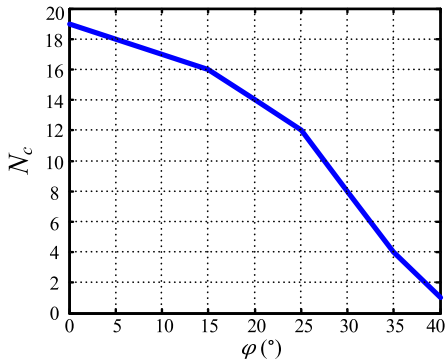

Fig. 11. Curve of N_c versus φ.

IV. Optimization on Coils and Phase-Shifted Angles for Stable Output Power

For MCR WPT systems, the output power with high amplitude and small fluctuation under large misalignment is always considered as a superior output power characteristic. As mentioned above, the output power is hard to be maintained at a constant level when the spatial position of the receiving coil changes, even though the phase-shifted angle is introduced between each phase. Therefore, the parameters of coils and the specific phase-shifted angle should be designed synthetically and deliberately to meet the requirement of stable output power within the full range of angular misalignment.

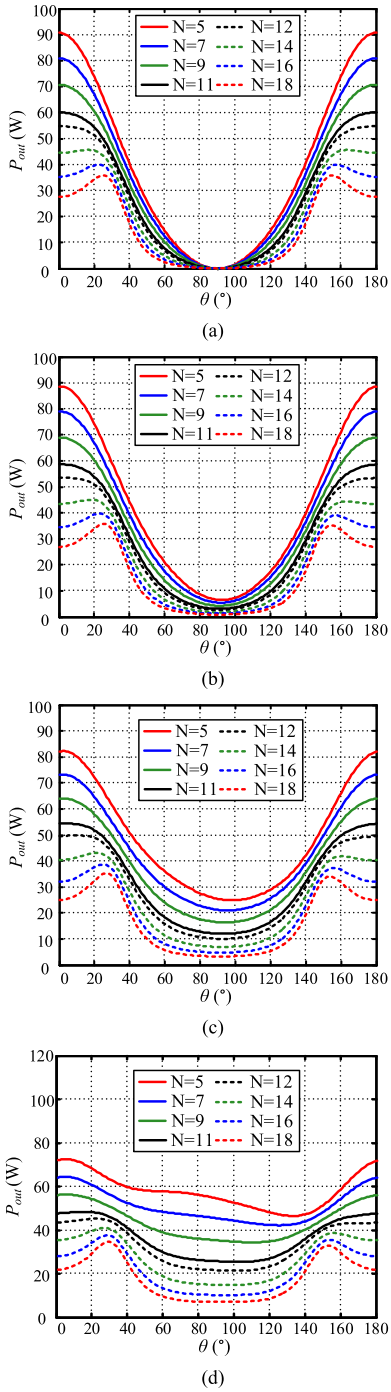

Fig. 12. Curves of output power against θ with different N, φ, and α. (a) $\varphi = 0°$, $\alpha = 0°$. (b) $\varphi = 10°$, $\alpha = 20°$. (b) $\varphi = 20°$, $\alpha = 40°$. (c) $\varphi = 30°$, $\alpha = 60°$.

Considering the previous assumption that coil turns $N_P = N_S = N$, M_x can be expressed by

$$M_x = N^2 \cdot M_{0x}. \tag{21}$$

Substituting (21) into (19), and then the relationship between the mutual inductance and the output power can be converted into the one between the coil turns and the output power. From (19), the output power is strictly related to φ, α, N, and θ. Fig. 12 shows the curves of output power as a function of θ and N with specific φ and α, where $\alpha = 2\varphi$ and the maximum φ is set at 30°

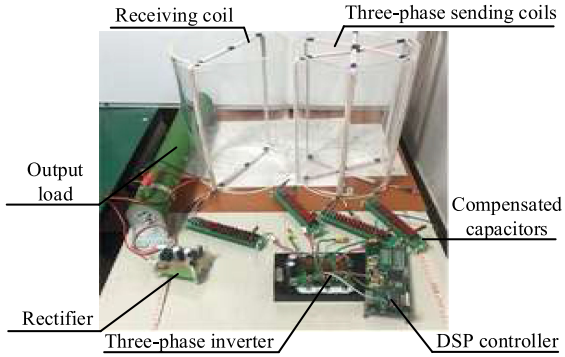

Fig. 13. Prototype of three-phase MCR WPT system.

to fulfill the ZVS requirement. By comparison among each subgraph, it can be known that the output power decreases initially and then increases along with the increasing θ in most cases. In Fig. 12(a), when $\varphi = \alpha = 0°$, the output power decreases to zero at $\theta = 90°$ and fluctuates widely regardless of N, which demonstrates that the stable output power cannot be realized in this case.

When φ increases, as illustrated in Fig. 12(b)–(d), the maximum and minimum output power are, respectively, lower and higher than the cases in Fig. 12(a) under same parameters, which means the fluctuation of output power decreases as expected. Comparing the subgraphs in Fig. 12(b)–(d), it can be concluded that the overall output power decreases along with the increasing N if φ and α are constant and the power fluctuation attenuates along with the increasing φ and α if N is constant. The optimal case obviously appears in Fig. 12(d), where the power fluctuation is minimum, and the output power shows nearly stable within the full range of angular misalignment by choosing an appropriate N. In this paper, the final optimal parameters are designed as $N = 7$, $\varphi = 30°$, and $\alpha = 60°$ according to Fig. 12(d).

V. Experimental Verifications

In order to validate the theoretical analysis, a prototype was built and tested in the laboratory, as shown in Fig. 13. To illustrate the superior performance of the optimized system and fulfill the comparison among the systems with different parameters, the experimental verification of two systems with and without optimized parameters ($N = 7$ and $N = 14$) are implemented, and the main specifications and coil parameters of the prototype are listed in Table I.

The measured experimental data of φ_P in three phases and φ_{PA} when $N = 14$ are plotted in Figs. 14 and 15 by dashed lines, along with the theoretical curves in solid lines. As shown, the experimental results are well in agreement with the theoretical curves, which validates the correctness of the simplified single-phase equivalent circuit model. From Figs. 14(a) and 15, the maximum φ_P increases along with φ when θ is constant, which presents the similar tendency as the theoretical analysis, meanwhile, all switches realize ZVS within the full range of angular misalignment when φ is designed between 0°∼30°.

Fig. 16 shows the key voltage and current waveforms in different cases. As shown in Fig. 16(a)–(c), the three-phase resonant currents are all sinusoidal waveforms, and their phase always lag to the corresponding driving signals, which means all switches can realize ZVS. However, in Fig. 16(d), when φ is larger than

TABLE I
PARAMETERS OF THE PROTOTYPE

Parameter	Symbol	Value	
Turns	N_P= N_S =N	7	14
Self-inductors	L_x	L_A=40.34 μH L_B=40.61 μH L_C=40.63 μH L_S=40.74 μH	L_A=142.12 μH L_B=143.02 μH L_C=145.82 μH L_S=142.67 μH
Compensated capacitors	C_x	C_A=62.8 nF C_B=62.4 nF C_C=62.3 nF C_S=62.2 nF	C_A=17.82 nF C_B=17.71 nF C_C=17.37 nF C_S=17.8 nF
Input voltage	V_{in}	72 V	
Operating frequency (Resonant frequency)	f_s (f_r)	100 kHz	
Transmission distance	D	25 cm	
Load resistance	R_L	5 Ω	

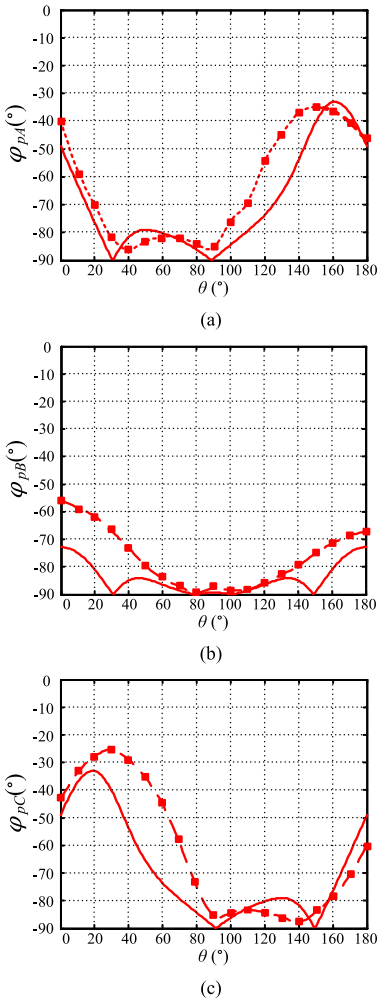

Fig. 14. Theoretical and experimental curves of φ_P when $\varphi = 0°$. (a) Phase *A*. (b) Phase *B*. (c) Phase *C*.

40°, the phase of i_C leads to the corresponding driving signal, which indicates the switches in phase *C* suffer hard switching.

Fig. 17 shows the output power with different coil turns and phase-shifted angles, in which, the measured experimental data are plotted by dashed lines, along with the theoretical curves in solid lines. It is also observed that the experimental results

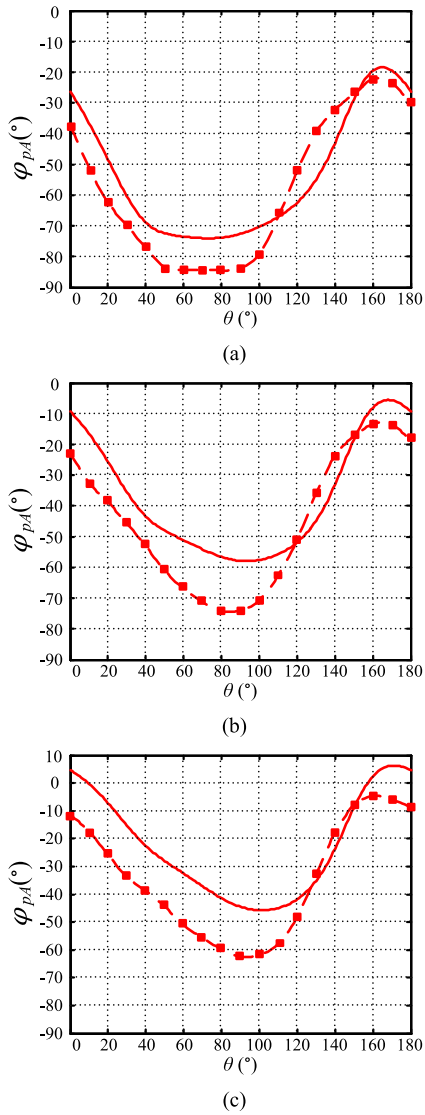

Fig. 15. Theoretical and experimental curves of φ_P in phase *A*. (a) $\varphi = 10°$. (b) $\varphi = 20°$. (c) $\varphi = 30°$.

match well with the theoretical one. Meanwhile, the overall output power level is improved when the coil turns are designed to be relatively small, and the increased phase-shifted angle contributes to reduce the fluctuation of output power. In addition, compared with the other cases, the system presents an optimal output power characteristic within full range of angular misalignment when $N = 7$, $\varphi = 30°$, and $\alpha = 60°$.

VI. CONCLUSION

In this paper, a three-phase MCR WPT system with cylinder-shaped coils that is suitable for the applications with arbitrary angular misalignment of loads was investigated. The FHA method was adopted to build the equivalent circuit model for the steady-state analysis. Based on the theoretical analysis, the parametric optimization of the coil turns and phase-shifted angles to achieve ZVS for the driver inverter and stable output power characteristics was carried out. To realize ZVS for the switches in the driver inverter within full range of angular misalignment, the

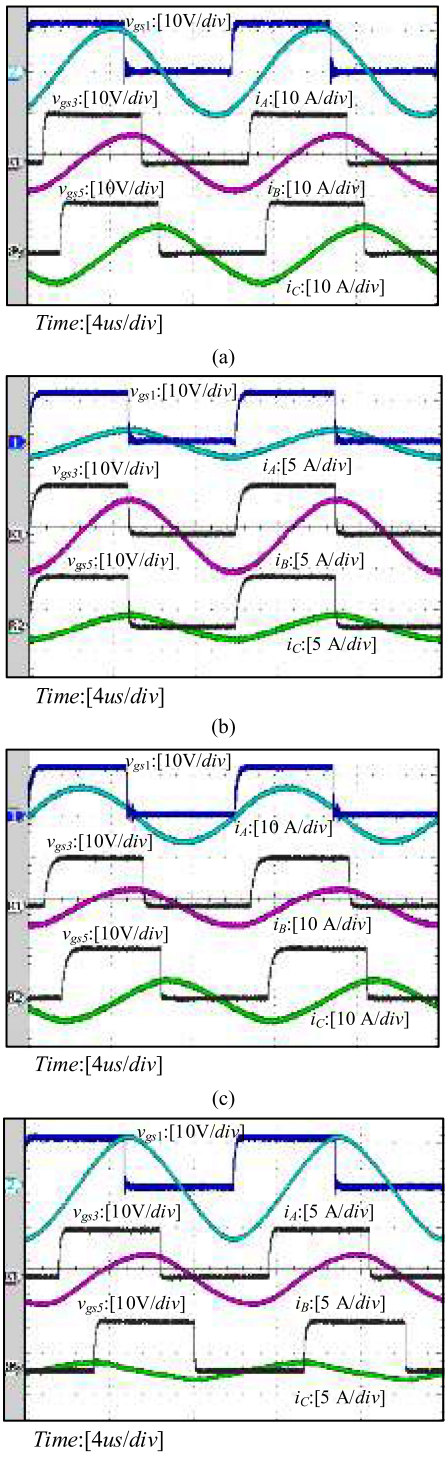

Fig. 16. Experimental waveforms. (a) $N = 7$, $\varphi = 30°$, $\alpha = 60°$, $\theta = 0°$. (b) $N = 14$, $\varphi = 0°$, $\alpha = 0°$, $\theta = 90°$. (c) $N = 14$, $\varphi = 30°$, $\alpha = 60°$, $\theta = 0°$. (d) $N = 14$, $\varphi = 60°$, $\alpha = 120°$, $\theta = 0°$.

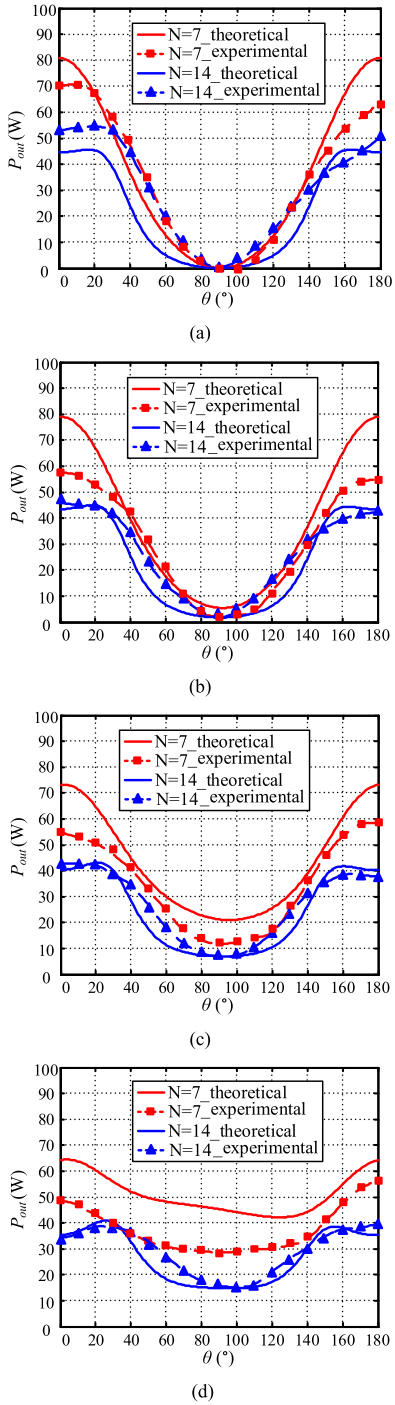

Fig. 17. Theoretical and experimental curves of P_{out}. (a) $\varphi = 0°$, $\alpha = 0°$. (b) $\varphi = 10°$, $\alpha = 20°$. (c) $\varphi = 20°$, $\alpha = 40°$. (d) $\varphi = 30°$, $\alpha = 60°$.

constraint between the phase-shifted angles should be $\alpha = 2\varphi$, and the maximum φ should be less than 40°. To further optimize the output power performance, the output power trends under different angular misalignments and system parameters were analyzed. It is found that small coil turns are conductive to enhance the overall output power level, and the output power can be maintained approximately at a constant value under specific coil turns and phase-shifted angles. To validate the theoretical analysis and feasibility of optimal design method, a prototype with two sets of parameters had been built and tested. The experimental results are well in agreement with the theoretical analysis, verifying the accuracy of the analytical model and the feasibility of the proposed optimization method.

REFERENCES

[1] S. Y. R. Hui, W. X. Zhong, and C. K. Lee, "A critical review on recent progress in mid-range wireless power transfer," *IEEE Trans. Power Electron.*, vol. 29, no. 9, pp. 4500–4511, Sep. 2014.

[2] N. Shinohara, "Wireless power transmission progress for electric vehicle in Japan," in *Proc. IEEE Radio Wireless Symp.*, 2013, pp. 109–111.

[3] G. A. Covic and J. T. Boys, "Inductive power transfer," *Proc. IEEE*, vol. 101, no. 6, pp. 1276–1289, Jun. 2013.

[4] S. Y. R. Hui and W. W. C. Ho, "A new generation of universal contactless battery charging platform for portable consumer electronic equipment," *IEEE Trans. Power Electron.*, vol. 20, no. 3, pp. 620–627, May 2005.

[5] A. Kurs, A. Karalis, R. Moffatt, J. D. Joannopoulos, P. Fisher, and M. Soljacic, "Wireless power transfer via strongly coupled magnetic resonances," *Science*, vol. 317, no. 5834, pp. 83–86, Jul. 2007.

[6] C. Y. Xiao, K. Z. Wei, D. N. Cheng, and Y. F. Liu, "Wireless charging system considering eddy current in cardiac pacemaker shell: Theoretical modeling, experiments, and safety simulations," *IEEE Trans. Ind. Electron.*, vol. 64 no. 5, pp. 3978–3988, May 2016.

[7] Z. G. Dang and J. A. A. Qahouq, "Modeling and investigation of magnetic resonance coupled wireless power transfer system with lateral misalignment," in *Proc. IEEE Appl. Power Electron. Conf.*, 2014, pp. 1317–1322.

[8] J. H. Wang *et al.*, "Lateral and angular misalignments analysis of a new PCB circular spiral resonant wireless charger," *IEEE Trans. Magn.*, vol. 48, no. 11, pp. 4522–4525, Nov. 2012.

[9] F. X. Liu, Y. Yang, D. Jiang, X. B. Ruan, and X. L. Chen, "Modeling and optimization of magnetically coupled resonant wireless power transfer system with varying spatial scales," *IEEE Trans. Power Electron.*, vol. 32, no. 4, pp. 3240–3250, Sep. 2017.

[10] K. Fotopoulou and B. W. Flynn, "Wireless power transfer in loosely coupled links: Coil misalignment model," *IEEE Trans. Magn.*, vol. 47, no. 2, pp. 416–430, Feb. 2011.

[11] W. M. Ng, C. Zhang, D. Y. Lin, and S. Y. R. Hui, "Two and three-dimensional omnidirectional wireless power transfer," *IEEE Trans. Power Electron. Lett.*, vol. 29, no. 9, pp. 4470–4474, Sep. 2014.

[12] D. Y. Lin, C. Zhang, and S. Y. R. Hui, "Mathematical analysis of omnidirectional wireless power transfer—Part-I: Two-dimensional systems," *IEEE Trans. Power Electron.*, vol. 32, no. 1, pp. 625–633, Jan. 2017.

[13] G. A. Covic, J. T. Boys, M. L. G. Kissin, and H. G. Lu, "A three-phase inductive power transfer system for roadway powered vehicles," *IEEE Trans. Ind. Electron.*, vol. 54, no. 6, pp. 3370–3378, Dec. 2007.

[14] H. Matsumoto, Y. Neba, K. Ishizaka, and R. Itoh, "Model for a three-phase contactless power transfer system," *IEEE Trans. Power Electron.*, vol. 26, no. 9, pp. 2676–2687, Sep. 2011.

[15] C. Zhang, D. Y. Lin, and S. Y. R. Hui, "Basic control principles of omnidirectional wireless power transfer," *IEEE Trans. Power Electron.*, vol. 31, no. 7, pp. 5215–5227, Jul. 2016.

[16] D. Y. Lin, C. Zhang, and S. Y. R. Hui, "Mathematical analysis of omnidirectional wireless power transfer—Part-II: Three-dimensional systems," *IEEE Trans. Power Electron.*, vol. 32, no. 1, pp. 613–624, Jan. 2017.

[17] O. Jonah, S. V. Georgakopoulos, and M. M. Tentzeris, "Orientation insensitive power transfer by magnetic resonance for mobile devices," in *Proc. IEEE Wireless Power Transfer*, 2013, pp. 5–8.

[18] T. Hosotani and I. Awai, "A novel analysis of ZVS wireless power transfer system using coupled resonators," in *Proc. IEEE Microw. Workshop Ser.*, 2012, pp. 235–238.

[19] H. Matsumoto, Y. Neba, H. Iura, D. Tsutsumi, K. Ishizaka, and R. Itoh, "Trifoliate three-phase contactless power transformer in case of winding-alignment," *IEEE Trans. Ind. Electron.*, vol. 61, no. 1, pp. 53–62, Jan. 2014.

[20] D. Jiang, Y. Yang, F. X. Liu, X. B. Ruan, and X. L. Chen, "Optimization of coils for magnetically coupled resonant wireless power transfer system based on maximum output power," in *Proc. IEEE Appl. Power Electron. Conf.*, 2016, pp. 1788–1794.

[21] L. Gao *et al.*, "Optimum design of coil for wireless energy transmission system based on resonant coupling," in *Proc. IEEE Int. Conf. Control Autom.*, 2013, pp. 190–195.

[22] H. C. Li, K. P. Wang, L. Huang, J. Li, and X. Yang, "Coil structure optimization method for improving coupling coefficient of wireless power transfer," in *Proc. IEEE Appl. Power Electron. Conf.*, 2015, pp. 2518–2521.

[23] C. Jiang, F. X. Liu, X. B. Ruan, and X. L. Chen, "Transmission characteristic analysis of a three-phase magnetically coupled resonant wireless power transfer system," in *Proc. IEEE Energy Conv. Cong. Expo.*, 2016, pp. 1–6.

Fuxin Liu (M'09–SM'16) was born in Heilongjiang Province, China, in 1979. He received the B.S., M.S., and Ph.D. degrees in electrical engineering from the Nanjing University of Aeronautics and Astronautics (NUAA), Nanjing, China, in 2001, 2004, and 2007, respectively.

In 2007, he joined the Faculty of the College of Automation Engineering, NUAA, where he is currently an Associate Professor. From 2018 to 2019, he joined the Department of Electrical and Computer Engineering, Technical University of Munich (TUM), Munich, Germany, and served as a Visiting Professor. His main research interests include wireless power transfer, soft-switching dc/dc converters, and renewable energy generation systems.

Dr. Liu was the recipient of the August-Wilhelm Scheer Visiting Professorship of TUM, TUM Ambassador, and serves as an Honorary Fellow of the TUM Institute for Advanced Study.

Ze Ding was born in Jiangsu Province, China, in 1996. He received the B.S. degree in electrical engineering and automation in 2017 from Nanjing University of Aeronautics and Astronautics, Nanjing, China, where he is currently working toward the M.S. degree in electrical engineering.

His main research interests include wireless power transfer.

Xiewei Fu was born in Hubei Province, China, in 1992. He received the B.S. and M.S. degrees in electrical engineering from Nanjing University of Aeronautics and Astronautics, Nanjing, China, in 2015 and 2018, respectively.

In 2018, he joined China Aerospace Science and Industry Corporation, Wuhan, China, where he is currently a Technical Engineer. His main research interests include wireless power transfer.

Ralph M. Kennel (M'89–SM'96) was born in Kaiserslautern, Germany, in 1955. He received the Diploma and Dr. Ing. (Ph.D.) degrees in electrical engineering from the University of Kaiserslautern, Kaiserslautern, Germany, in 1979 and 1984, respectively.

From 1983 to 1999, he worked on several positions with Robert BOSCH GmbH (Germany). Until 1997, he was responsible for the development of servo drives. From 1994 to 1999, he was a Visiting Professor with the University of Newcastle-upon-Tyne, Newcastle-upon-Tyne, U.K. From 1999 to 2008, he was a Professor of electrical machines and drives with Wuppertal University, Wuppertal, Germany. Since 2008, he has been a Professor of electrical drive systems and power electronics with Technical University of Munich, Munich, Germany. His current main interests include renewable energy systems, sensorless control of ac drives, predictive control of power electronics, and hardware-in-the-loop systems.

Dr. Kennel is a Fellow of the IEE and a Chartered Engineer in the U.K. within IEEE, he is a Treasurer of the Germany Section as well as ECCE Global Partnership Chair of the Power Electronics society. He is an Associate Editor for the IEEE TRANSACTIONS ON POWER ELECTRONICS.